ANODIC OXIDATION OF NOVEL HOLE-TRANSPORTING MATERIALS DERIVED FROM TETRAARYLBENZIDINES. ELECTROCHEMICAL AND SPECTROSCOPIC CHARACTERIZATION

René FÁBER[a1,b], G. Felix MIELKE[b1], Peter RAPTA[a2], Andrej STAŠKO[a3,*] and Oskar NUYKEN[b2]

[a] *Department of Physical Chemistry, Slovak Technical University, Radlinského 9, SK-812 37 Bratislava, Slovak Republic; e-mail:* [1] *rene.faber@ch.tum.de,* [2] *rapta@cvt.stuba.sk,* [3] *stasko@cvt.stuba.sk*

[b] *Lehrstuhl für Makromolekulare Stoffe, Technische Universität München, Lichtenbergstr. 4, D-85747 Garching, Germany; e-mail:* [1] *felix.mielke@ch.tum.de,* [2] *oskar.nuyken@ch.tum.de*

Received March 15, 2000
Accepted June 16, 2000

Dedicated to Professor Ľudovít Treindl in honour of his 70th birthday.

Fluorenylidene-linked triarylamines, potential hole-transporting materials, have been prepared by the palladium-catalyzed Hartwig–Buchwald amination. Their redox and spectral properties were investigated in solution, applying cyclic voltammetry, UV-VIS and EPR spectroscopy, and *in situ* spectroelectrochemical measurements. *N*,*N*,*N*′,*N*′-Tetraphenylbenzidine (**1**), *N*,*N*′-di(1-naphthyl)-*N*,*N*′-diphenylbenzidine (**2**), and triphenylamine (**3**) served as model substances in the study of the synthesized complex compounds **4** and **5**. In structure **4**, two triphenylamine centres are linked with a non-conjugated fluorene bridge; in structure **5**, two tetraarylbenzidine skeletons with two nitrogens are linked with a conjugated biphenyl-bridge system. In addition, structure **5** contains a non-conjugated fluorene bridge. The presence of the fluorene moiety in the molecular design has a significant influence on the investigated properties of the new materials. In the anodic oxidation of the tetraarylbenzidine-type compounds (**1**, **2**, and **5**), two well-defined reversible oxidation peaks were observed. However, the oxidation of the triphenylamine-type structures (**3** and **4**) is more complex, due to fast consecutive reactions. The dimer-like structures (**4** and **5**) are characterized by two independent oxidation centres that are simultaneously oxidized at approximately the same potentials. This was confirmed by quantitative cyclovoltammetric as well as UV-VIS investigations.

Key words: EPR/UV-VIS spectroelectrochemistry; Cyclic voltammetry; Hole-transporting materials; Tetraarylbenzidines; Hartwig–Buchwald amination; Triarylamines; Electrochemistry.

Organic hole-transporting materials find applications in organic light-emitting diodes (OLEDs)[1]. To be candidates for the use in hole-transporting layers, organic materials should possess a variety of

chemical and physical properties, such as good electrochemical stability, a low ionisation potential, reversible redox behaviour, hole-transport and hole-injection ability from the anode into the hole-transporting layer (HTL). In addition, thermal stability, photostability, and good film-forming properties are required. At present, triphenylamine derivatives are commonly used as hole-transporting materials, usually in the form of tetraarylbenzidines[2–4]. However, these compounds suffer from low thermal stability because of their low glass-transition temperatures. Several approaches were considered to improve the thermal properties of triarylamine HTL materials, such as synthesis of "starburst" molecules[5,6], asymmetric substitution of benzidine derivatives[7,8], or the use of spiro linkages[9–11]. Low-molecular-weight triarylamines have also been incorporated into polymers[12].

In this work, we present a new concept for increasing the glass-transition temperature (T_g) of OLED materials. The aim is to couple two hole-transporting units in a way that thermal and film-forming properties are improved while the electronic characteristics are not impaired. This can be achieved by a rigid linker that increases molecular weight and steric demands but does not lead to a conjugated system of the hole-transporting subunits. As a linker, we chose the sp^3-carbon of fluorene. The resulting diphenylfluorene structure has been shown to increase T_g and solubility in polymers with rigid aromatic structures[13,14]. Since the fluorene unit and the two phenyl rings are not conjugated, this linkage should preserve the favourable electronic characteristics of the low-molecular-weight triarylamines.

Therefore we investigated low-molecular-weight materials, *N*,*N*,*N*′,*N*′-tetraphenylbenzidine (TPB) (**1**), *N*,*N*′-di(1-naphthyl)-*N*,*N*′-diphenylbenzidine (α-NPD) (**2**), and triphenylamine (TPA) (**3**) as model substances to estimate redox and spectral properties of the newly synthesized compounds F-TPA (**4**) and F-1αNPD (**5**) shown in Scheme 1. The hole-transporting and electrochemical properties of compounds **1–3** have already been described, and they have also been employed in OLEDs[3,15–22].

The synthesis of **4** by the Ullmann coupling and its characteristics as a hole-transporting layer in OLEDs have been reported by Okutsu *et al.*[23]. In our work, we used a tetraarylbenzidine derivative as a hole-transporting unit which leads to an electrochemical potential more suitable for applications of OLEDs. Compounds **4** and **5** were prepared using the palladium-catalyzed Hartwig–Buchwald amination of bromoarenes[24–26] (Scheme 2). Morphological instability under operating conditions is assumed to be one of the most important failure modes of OLEDs, the problem that can be

overcome by higher T_g of materials. The new compound **5** has a T_g of 153 °C which is one of the highest reported for the triarylamines so far used in OLEDs (refs[8,26-29]).

The ionization potential of hole-transporting layers is a crucial factor in molecular design of hole-transport materials suitable for producing electroluminescent (EL) devices of high durability. In particular, the formation of a small energy barrier at the HTL/anode interface is essential for high durability.

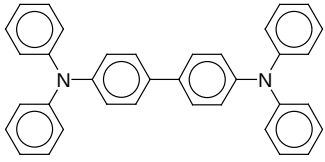

1 (TPB)

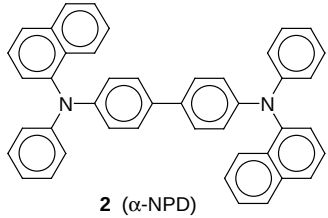

2 (α-NPD)

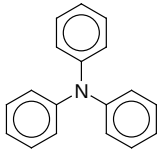

3 (TPA)

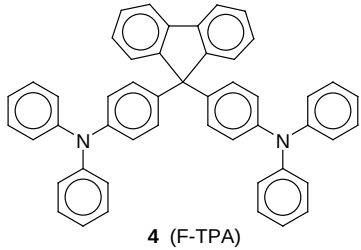

4 (F-TPA)

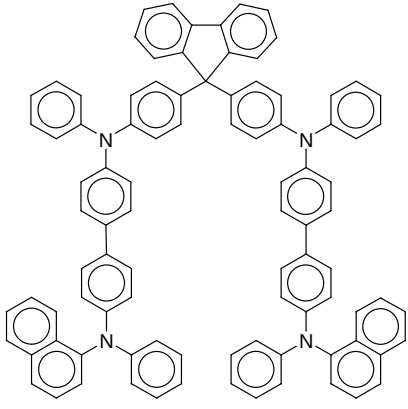

5 (F-1αNPD)

SCHEME 1

The aim of this contribution is to determine redox properties of the newly synthesized compounds **4** and **5**, including the charge-injection barrier of the hole-transport materials with respect to indium-tin-oxide (ITO). The evaluation of their HOMO energies based on cyclovoltammetric measurements, using the ferrocene/ferrocenium internal redox standard[30]. In order to find a plausible mechanism of the oxidation of **4** and **5**, our cyclovoltammetric studies were completed with *in situ* EPR and UV-VIS spectroelectrochemical investigations.

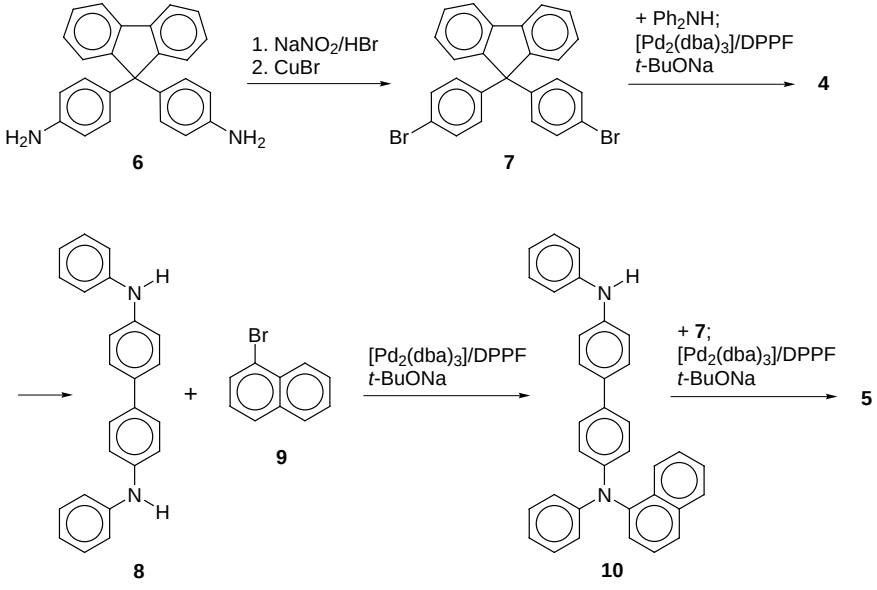

SCHEME 2

EXPERIMENTAL

Instrumentation

The cyclic voltammograms were recorded using a platinum wire as working and auxiliary electrodes. A saturated calomel electrode (SCE) served as reference. The measurements were carried out with a Princeton Applied Research (PAR 270) universal electrochemical system. Ferrocene/ferricenium (Fc/Fc^+) was used as an internal potential marker.

Laminated gold-μ-mesh[31], or laminated conducting ITO coated glass-plate electrodes[32] were employed in spectroelectrochemical experiments. Redox cycling of the investigated compounds with simultaneous EPR and UV-VIS measurements was carried out in dichloromethane solutions containing 0.1 M tetrabutylammoniumhexafluorophosphate ($TBAPF_6$). The reference electrode consisted of a silver wire coated with silver chloride. EPR spectra

were recorded on an ESR 200D X-Band spectrometer (Bruker, Germany). UV-VIS spectra (λ in nm) were recorded on a diode array UV-VIS spectrophotometer PC 1000 (Ocean Optics, Inc.). A HEKA PG 284 (Lambrecht, Germany) potentiostat/galvanostat was used as electrochemical equipment for these measurements.

Since no changes in the shape of the EPR spectra were observed during the redox cycling, the intensity of the EPR signal was also recorded using constant-field conditions. The magnetic field was set on the maximal intensity of the EPR line of the investigated radical intermediate and the EPR intensity was measured in a time-based mode.

Materials

9,9-Bis(4-aminophenyl)fluorene, triphenylamine, diphenylamine, 1-bromonaphthalene, 1,1′-bis(diphenylphosphino)ferrocene (DPPF), and sodium *tert*-butoxide were purchased from Aldrich; hydrobromic acid, *N*,*N*′-diphenylbenzidine, tetrabutylammoniumhexafluorophosphate and dichloromethane from Fluka; *N*,*N*,*N*′,*N*′-tetraphenylbenzidine from SynTec (Wolfen, Germany); tris(dibenzylideneacetone)dipalladium(0) ($Pd_2(dba)_3$) and palladium acetate from Strem Chemicals. All chemicals were used as received.

Syntheses

All palladium-catalyzed reactions were carried out in dried solvents under nitrogen.

N,*N*′-Di(1-naphthyl)-*N*,*N*′-diphenylbenzidine[33] (**2**)

To a stirred solution of palladium acetate (90 mg, 400 μmol) and 1,1′-bis(diphenylphosphino)ferrocene (222 mg, 400 μmol) in toluene (100 ml) were added *N*,*N*′-diphenylbenzidine (3.36 g, 10.0 mmol) and 1-bromonaphthalene (6.21 g, 30.0 mmol). After addition of sodium *tert*-butoxide (2.31 g, 24.0 mmol), the mixture was refluxed under nitrogen for 3 days. After cooling, 100 ml of brine were added and the mixture was extracted twice with chloroform. The combined organic phases were washed with brine and dried over anhydrous magnesium sulfate. The solvents were removed on a rotary evaporator, and the residue was purified by column chromatography on silica gel using cyclohexane–toluene (4 : 1 v/v) as eluent. Yield 3.17 g (54%). MS, *m/z* (%): 588 (M^+, 100), 294 (M^{2+}, 22), 217 (8). ^{1}H NMR ($CDCl_3$): 7.94 (m, 2 H); 7.87 (m, 2 H); 7.76 (m, 2 H); 7.52–7.25 (m, 12 H); 7.19 (m, 4 H); 7.08–6.87 (m, 10 H). ^{13}C NMR ($CDCl_3$): 148.35, 147.27, 143.47, 135.30, 133.84, 131.27, 129.10, 128.38, 127.23, 127.08, 126.48, 126.39, 126.35, 126.13, 124.29, 121.96, 121.92, 121.73. For $C_{44}H_{32}N_2$ (588.8) calculated: 89.76% C, 5.48% H, 4.76% N; found: 89.73% C, 5.45% H, 4.69% N.

9,9-Bis(4-bromophenyl)fluorene **(7)**

9,9-Bis(4-aminophenyl)fluorene (3.49 g, 10.0 mmol) was suspended in 35% aqueous hydrobromic acid (35 ml) and the suspension was cooled to 0 °C. Ice-cold 2.5 M $NaNO_2$ solution (8 ml) was added dropwise so that the temperature did not rise above 5 °C. The yellow suspension was added to a solution of CuBr (2.00 g, 14.0 mmol) in 48% aqueous hydrobromic acid (10 ml) at 0 °C. After stirring for 5 min, the mixture was heated to 100 °C until the formation of gas ceased. After cooling, the mixture was extracted with chloroform three times (20 ml each). The combined organic phases were washed with brine and dried

over anhydrous magnesium sulfate. The solvent was removed on a rotary evaporator. The residue was purified by column chromatography on silica gel using cyclohexane as eluent. Yield 3.24 g (68%). MS, *m/z* (%): 476 (M^+, 100), 397 (27), 395 (28), 321 (26), 319 (27), 315 (14), 239 (55), 198.5 (14), 197.5 (15). ^{1}H NMR ($CDCl_3$): 7.76 (m, 2 H); 7.45–7.22 (m, 10 H); 7.04 (m, 4 H). ^{13}C NMR ($CDCl_3$): 150.16, 144.53, 140.07, 131.44, 129.78, 127.99, 127.93, 125.85, 120.95, 120.42, 64.61. For $C_{25}H_{16}Br_2$ (476.2) calculated: 63.06% C, 3.39% H, 33.56% Br; found: 63.27% C, 3.37% H, 33.43% Br.

9,9-Bis[4-(diphenylamino)phenyl]fluorene (**4**)

To a stirred solution of tris(dibenzylideneacetone)dipalladium(0) (37 mg, 40 μmol) and 1,1′-bis(diphenylphosphino)ferrocene (44 mg, 80 μmol) in toluene (20 ml) were added 9,9-bis(4-bromophenyl)fluorene **7** (952 mg, 2.0 mmol) and diphenylamine (745 mg, 4.4 mmol). After addition of sodium *tert*-butoxide (463 mg, 4.8 mmol) the mixture was refluxed under nitrogen for 24 h. After cooling, 50 ml of brine were added and the mixture was extracted twice with dichloromethane. The combined organic phases were washed with brine and dried over anhydrous magnesium sulfate. The solvents were removed on a rotary evaporator, and the residue was purified by column chromatography on silica gel using cyclohexane–toluene (2 : 1 v/v) as eluent. Yield 675 mg (52%). MS, *m/z*: 652 (M^+, 100), 408 (25), 326 (M^{2+}, 32). ^{1}H NMR ($CDCl_3$): 7.74 (m, 2 H); 7.43 (m, 2 H); 7.34 (m, 2 H); 7.27 (m, 2 H); 7.19 (m, 8 H); 7.08–7.01 (m, 12 H); 6.96 (m, 4 H); 6.89 (m, 4 H). ^{13}C NMR ($CDCl_3$): 151.56, 147.68, 146.15, 140.05, 139.73, 129.14, 128.87, 127.57, 127.35, 126.23, 124.32, 123.11, 122.69, 120.09, 64.50. For $C_{49}H_{36}N_2$ (652.8) calculated: 90.15% C, 5.56% H, 4.29% N; found: 89.59% C, 5.68% H, 4.06% N.

N-(1-Naphthyl)-*N*,*N*′-diphenylbenzidine (**10**)

To a stirred solution of palladium acetate (45 mg, 200 μmol) and 1,1′-bis(diphenylphosphino)ferrocene (111 mg, 200 μmol) in toluene (150 ml) were added *N*,*N*′-diphenylbenzidine (6.06 g, 18.0 mmol) and 1-bromonaphthalene (1.255 g, 6.0 mmol). After addition of sodium *tert*-butoxide (692 mg, 7.2 mmol), the mixture was refluxed under nitrogen for 46 h. After cooling, 300 ml of toluene and 100 ml of brine were added, and excess *N*,*N*′-diphenylbenzidine was filtered off. The aqueous phase was extracted with toluene (100 ml). The organic phases were combined, washed with brine and dried over anhydrous magnesium sulfate. The solvents were removed on a rotary evaporator, and the residue was purified by column chromatography on silica gel using cyclohexane–toluene (3 : 2 v/v) as eluent. Yield 1.124 g (40%). MS, *m/z* (%): 462 (M^+, 100), 231 (M^{2+}, 22). ^{1}H NMR (THF-d_8): 7.97 (m, 1 H); 7.90 (m, 1 H); 7.79 (m, 1 H); 7.52–7.30 (m, 9 H); 7.23–6.98 (m, 12 H); 6.89 (m, 1 H); 6.80 (m, 1 H). ^{13}C NMR (THF-d_8): 149.77, 148.21, 144.93, 144.80, 144.00, 136.70, 135.73, 133.40, 132.48, 129.98, 129.40, 128.14, 127.98, 127.74, 127.39, 127.28, 127.21, 127.04, 125.26, 123.27, 122.81, 122.56, 120.97, 118.34 (2 C). For $C_{34}H_{26}N_2$ (462.6) calculated: 88.28% C, 5.66% H, 6.06% N; found: 88.29% C, 5.62% H, 5.69% N.

9,9-Bis[4-(*N*-{4′-[*N*-(1-naphthyl)anilino]biphenyl-4-yl}anilino)phenyl]fluorene (**5**)

To a stirred solution of tris(dibenzylideneacetone)dipalladium(0) (69 mg, 75 μmol) and 1,1′-bis(diphenylphosphino)ferrocene (83 mg, 150 μmol) in toluene (40 ml) were added 9,9-bis(4-bromophenyl)fluorene (**7**; 1.19 g, 2.5 mmol) and *N*-(1-naphthyl)-*N*,*N*′-diphenyl-

benzidine (**10**; 2.31 g, 5.0 mmol). After addition of sodium *tert*-butoxide (577 mg, 6.0 mmol), the mixture was refluxed under nitrogen for 6 days. After cooling, 50 ml of brine was added, and the mixture was extracted three times with chloroform. The organic phases were combined, washed with brine and dried over anhydrous magnesium sulfate. The solvents were removed on a rotary evaporator, and the residue was purified by column chromatography on silica gel using cyclohexane–chloroform (1 : 1 v/v) as eluent. Yield 2.00 g (65%). MS (MALDI-TOF), *m/z* (%): 1 239 (M^+, 100). ^{1}H NMR ($CDCl_3$): 7.94 (m, 2 H); 7.87 (m, 2 H); 7.74 (m, 4 H); 7.49–7.13 (m, 30 H); 7.09–6.87 (m, 28 H). ^{13}C NMR ($CDCl_3$): 151.53, 148.28, 147.56, 147.36, 146.40, 146.03, 143.43, 140.04, 139.81, 135.28, 134.83, 133.69, 131.24, 129.17, 129.10, 128.90, 128.38, 127.59, 127.35, 127.22, 127.14 (2 C); 126.48, 126.39, 126.34, 126.23, 126.13, 124.43, 124.26 (2 C); 123.21, 122.80, 122.00, 121.82, 121.78, 120.09, 64.51. For $C_{93}H_{66}N_4$ (1 239.6) calculated: 90.11% C, 5.37% H, 4.52% N; found: 89.56% C, 6.07% H, 4.07% N.

RESULTS AND DISCUSSION

A characteristic feature of structures **1**, **2**, and **5** is the tetraarylbenzidine skeleton, where two nitrogen centres are linked by a conjugated biphenyl bridge. In addition, structure **5** contains a non-conjugated fluorene bridge. The characteristic structure of compounds **3** and **4** is a skeleton centred around only one nitrogen atom (triphenylamine in **3** and two triphenylamines linked by a non-conjugated fluorene bridge in **4**). These attributes are strongly reflected in the results obtained.

The cyclic voltammograms of the "tetraarylbenzidine" structures **2** and **5** with biphenyl-conjugated bridges are shown in Figs 1a-1 and 1b-1, respectively. In both cases two chemically reversible oxidations were observed. The extracted data (peak and half-wave potentials, and peak-to-peak separations) are summarized in Table I.

TABLE I
Peak and half-wave potentials, and peak separations extracted from cyclic voltammograms of compounds **1**–**5** (in V *vs* SCE, scan rate 100 mV s^{-1}) measured in 0.001 M solutions of substrate and 0.1 M solutions of $TBAPF_6$ in CH_2Cl_2

Compound	E^1_{pa}	E^2_{pa}	E^2_{pc}	E^1_{pc}	$E^1_{1/2}$	$E^2_{1/2}$	$\Delta E^{1,2}_p$
1	0.719	0.957	0.858	0.619	0.669	0.908	0.238
2	0.733	1.002	0.896	0.626	0.680	0.949	0.269
3	–	1.012[a]	0.859	0.642	–	–	–
4	–	0.982[a]	0.840	0.640	–	–	–
5	0.762[a]	1.011[a]	0.898[a]	0.646[a]	0.704	0.955	0.249

[a] Transfer of two electrons.

The half-wave potentials for the first oxidation of the tetraarylbenzidine structures (**1**, **2**, and **5**) are fairly similar, and centred at approximately 0.69 V *vs* SCE. The second oxidation occurs at about 0.93 V. These processes correspond to the formation of corresponding mono- and dications, respectively, as was reported[3,15] for **1** and **2**. However, as compound **5** contains two tetraarylbenzidine redox centres linked by a non-conjugated fluorene moiety, we also carried out spectroelectrochemical investigations in order to clarify the mechanism of the oxidation in this case. Therefore, our cyclovoltammetric studies were performed along with the EPR and UV-VIS investigations. The corresponding EPR spectra obtained at the potentials of the initial oxidation of **2** and **5** are presented in Figs 1a-2 and 1b-2, respectively. From the simulation of the EPR spectra of $\mathbf{1}^{+\bullet}$ and $\mathbf{2}^{+\bullet}$, the following

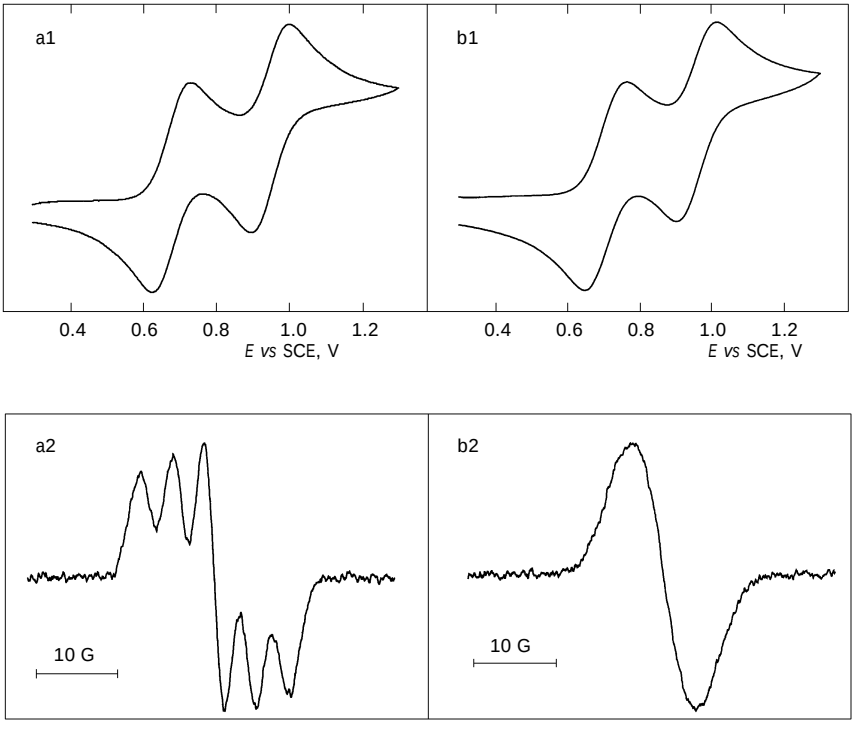

FIG. 1
Cyclic voltammograms of **2** (a-1) and **5** (b-1) showing oxidation in CH_2Cl_2/0.1 M $TBAPF_6$ (Pt working electrode, scan rate 100 mV s^{-1}), along with the EPR spectra of the corresponding cation-radicals of **2** (a-2) and **5** (b-2) generated in the potential region of the first anodic peaks

hyperfine splitting constants were obtained: $2a_N$(**1**) = 0.433 mT and $2a_N$(**2**) = 0.415 mT. This is in good agreement with the data reported for *N*,*N*′-bis-(3-methyl)-*N*,*N*′-diphenylbenzidine[34] (TPD). It is noteworthy that the EPR spectrum of compound **5** does not show any hyperfine splitting (see below).

Compounds **3** and **4** showed a completely different cyclovoltammetric behaviour. Only one partly reversible oxidation in the potential region of the second anodic peak (referring to the previous group of compounds) was observed, together with a small cathodic peak due to a secondary oxidation product on the reverse scan, as presented in Figs 2a-1 (**3**) and 2b-1 (**4**). This indicates that redox processes are associated with consecutive chemical reactions. In accordance with that assumption, the new redox couples are evident after the first anodic sweep with both compounds **3** and **4** (dashed lines in Figs 2a-1 and 2b-1) in the potential region from +0.6 to +0.8 V. Similar voltammograms were previously observed for model compound **3** (ref.[16]). Corresponding *in situ* EPR spectroelectrochemical experiment at the anodic potential around 1 V led to the EPR spectra shown in Figs 2a-2 and 2b-2 for **3** and **4**, respectively. The EPR spectrum in Fig. 2a-2 due to oxidized **3** corresponds to a radical centred with two equivalent nitrogens having the splitting constant $2a_N$ = 0.479 mT; additionally, well-resolved hyperfine splitting is evident. Analogously to the situation with **5**, oxidation of **4** only results in an unresolved broad EPR signal. The redox potentials of the new couples along with the splitting constants of two equivalent nitrogens strongly suggest the formation of a tetraphenylbenzidine skeleton, analogous to structures **1**, **2**, and **5**.

The cyclovoltammetric and EPR results obtained may be interpreted in the following way. The isolated triphenylamine skeleton in **3** is oxidized at high potentials (in the region of the second peak of tetraarylbenzidines) and forms cation-radicals, which rapidly dimerize under the formation of tetraphenylbenzidine. Consequently, a mixture of the EPR spectra characteristic of tetraarylbenzidine and triphenylamine cation-radicals is found. The observation of a well-resolved hyperfine splitting from hydrogen and nitrogen atoms here can be explained by the simultaneous presence of both cation-radicals. The EPR spectrum presented in Fig. 2a-2 was successfully simulated using the splitting parameters of $\mathbf{3}^{+\bullet}$ (a_N = 1.017 mT, $6a_H^o$ = 0.226 mT, $6a_H^m$ = 0.122 mT and $3a_H^p$ = 0.327 mT) and of $\mathbf{1}^{+\bullet}$ ($2a_N$ = 0.479 mT), assuming approximately equal relative EPR intensities and *g*-values of both species[35]. In addition, in the corresponding *in situ* UV-VIS spectroelectrochemical experiment, the formation of both mono- and dications derived from **1** as well as the formation of triphenylamine cation-radical were confirmed, as

will be discussed below. In agreement with that, the reverse cathodic peak at 0.64 V in Fig. 2 (a-1, b-1) can be assigned to the reduction of the monocation of the consecutively formed dimeric form (tetraphenylbenzidine). Similarly, the formation of tetraarylbenzidines was also reported[16,18–22]. We confirmed this dimerization process by having performed *in situ* UV-VIS electrochemical oxidation. Similar redox behaviour of compounds **3** and **4** suggests that a mechanism analogous to the oxidation route as found for **3** can also be assumed in the case of **4**.

Whereas the nature of the cation-radicals of compounds **1**, **2**, and **3** is evident from the EPR hyperfine structure, the issue is more complex in the case of the synthesized compounds **4** and **5**, where only a broad line was found. The fundamental difference between compounds **1–3** and **4**, **5** is

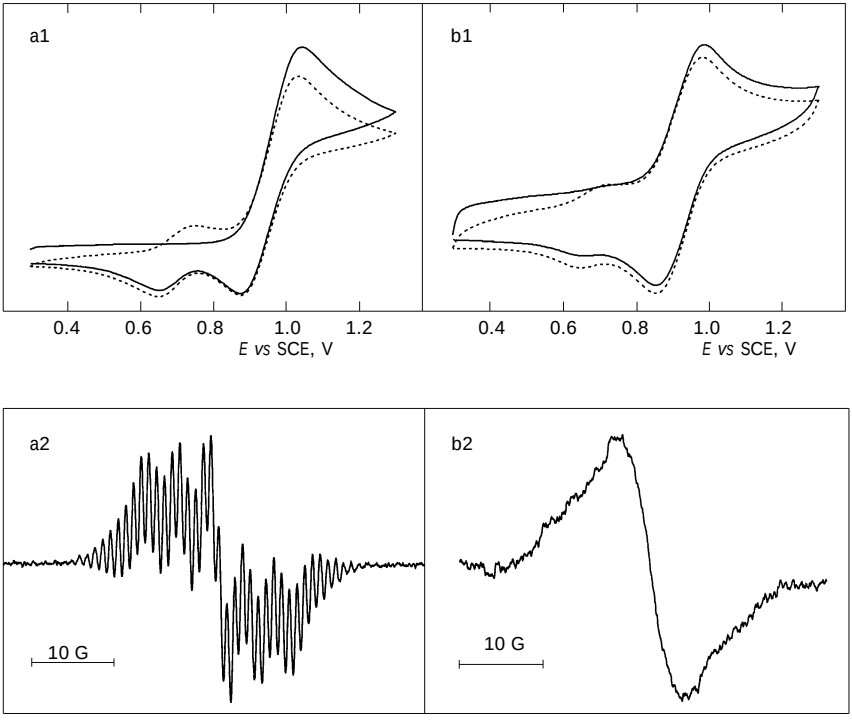

FIG. 2

Cyclic voltammograms of **3** (a-1) and **4** (b-1) showing oxidation in CH_2Cl_2/0.1 M $TBAPF_6$ (Pt working electrode, scan rate 100 mV s^{-1}, full line: first scan, dashed line: second scan), along with the EPR spectra of the cation-radicals generated in the potential region around 1 V during oxidation of **3** (a-2) and **4** (b-2)

that the former contain only one redox unit (tetraarylbenzidine in **1** and **2** or triphenylamine in **3**) while the latter contain two such units linked by a non-conjugated bridge (quaternary carbon of the fluorene moiety). We assume that the dimer-like structures behave as two independent oxidation centres and are very probably simultaneously oxidized at approximately the same potentials. This is indicated by the closely similar cyclic voltammograms for **2** and **5** with virtually the same positions of the oxidation peaks. Further evidence for this assumption is that at equivalent molar concentrations, the height of the peaks in the case of **5** is approximately double compared with that of **2,** as illustrated in Fig. 3a. Strong evidence for the simultaneous oxidation of both units in structures **4** and **5** comes from UV-VIS investigations. The UV-VIS spectrum of **5** exhibits approximately double the intensity of that of **2** at the same molar concentrations, as illustrated in Fig. 3b. Also, the EPR spectra are compatible with this assumption; as in the case of dimeric structures, the presence of two delocalized spins leads to collapse of the hyperfine structure accompanied by narrowing of the line.

All the compounds studied showed during oxidation similar UV-VIS bands in the region 300–800 nm. A precise attribution of the recorded UV-VIS spectra to the applied potential was possible from a simultaneous UV-VIS/cyclovoltammetric experiment.

Figure 4 shows a representative UV-VIS spectrocyclovoltammogram for compound **1**. Before oxidation, all starting compounds **1**–**5** have absorption

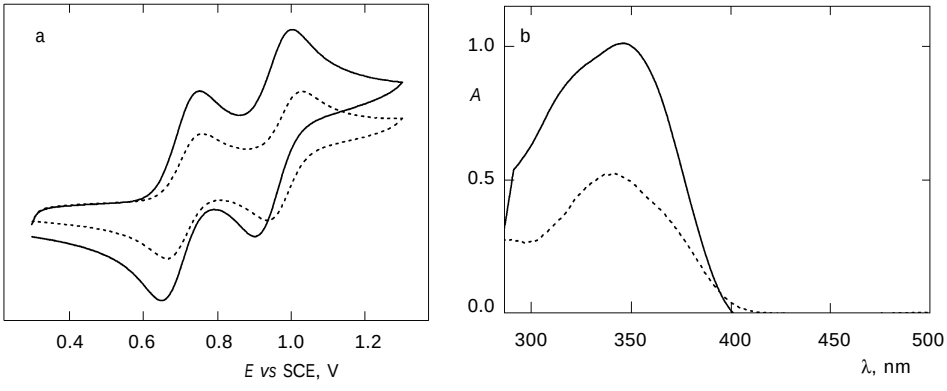

FIG. 3
Cyclic voltammograms (a) and UV-VIS spectra (b) of **2** (dashed lines) and **5** (full lines) measured in CH_2Cl_2/0.1 M $TBAPF_6$ at the same concentrations (0.001 mol l^{-1})

maxima in the region of 300–350 nm, and compound **1**, in addition, has a shoulder around 310 nm. The UV-VIS spectra were recorded simultaneously with a CV scan at the potentials marked with circles in the cyclic voltammogram, as illustrated in Fig. 4a. From Fig. 4 it is evident that the absorption band at 480 nm corresponds to the first oxidation peak of the monocation. At higher potentials, in the region of the second peak, the UV-VIS bands at 550–800 nm, which are attributed to the dication, predominate. Also the original VIS band at 480 nm reappears after dropping the potential to the region of the first oxidation peak.

More evidence for this assignment, also for the dimer-like structure **5**, was obtained from a simultaneous EPR/UV-VIS electrochemical study using a laminated ITO working electrode. Figure 5 (representative for compounds **1**, **2**, and **5**) shows the UV-VIS (Figs 5a, 5c) and also the upper half part of the EPR spectra (Fig. 5d) of compound **5**, that are simultaneously measured during the anodic (galvanostatic) oxidation on ITO in the cavity of the EPR spectrometer. During oxidation, the basic band (300–350 nm) of the parent compounds vanishes, and a new band arises with an isosbestic point at 392 nm. During further oxidation the monocation band passes through a maximum and is continuously replaced with a new band in the region 600–800 nm, again with an isosbestic point (at 530 nm). The kinetic curves extracted from the given UV-VIS spectra are shown in Fig. 5b. This kinetic behaviour is characteristic of two reversible one-electron oxidation processes. With the band increase in the range 550–800 nm, the intensity of

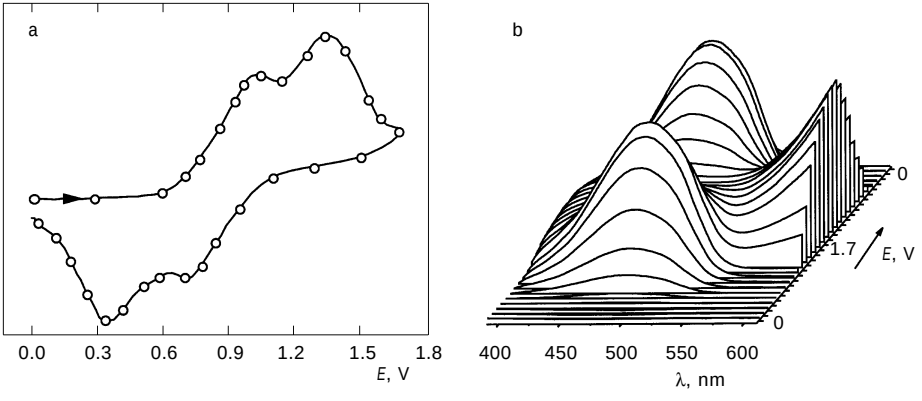

FIG. 4

Cyclic voltammogram (a) and UV-VIS spectra (b) recorded during a cyclovoltammetric scan at the potentials marked with circles (laminated ITO working electrode, scan rate 10 mV s^{-1})

the EPR line decreased. Therefore we assume that both redox centres of the two tetraarylbenzidine skeletons in **5** (linked with the non-conjugated fluorene bridge) are oxidized independently to the dication. An interesting observation is that after stopping the oxidation in the region of the second peak (550–800 nm) the intensity of EPR signal increases, indicating an increased concentration of monocation. This suggests a comproportionation reaction of the dication with the neutral tetraarylbenzidine in solution near the active electrode surface.

As specified above, the different behaviour in the cyclovoltammetric investigations of **3** and **4** was also reflected in *in situ* UV-VIS spectroelectrochemical experiments. During the oxidation, three new bands were observed simultaneously while the original band vanished as shown for

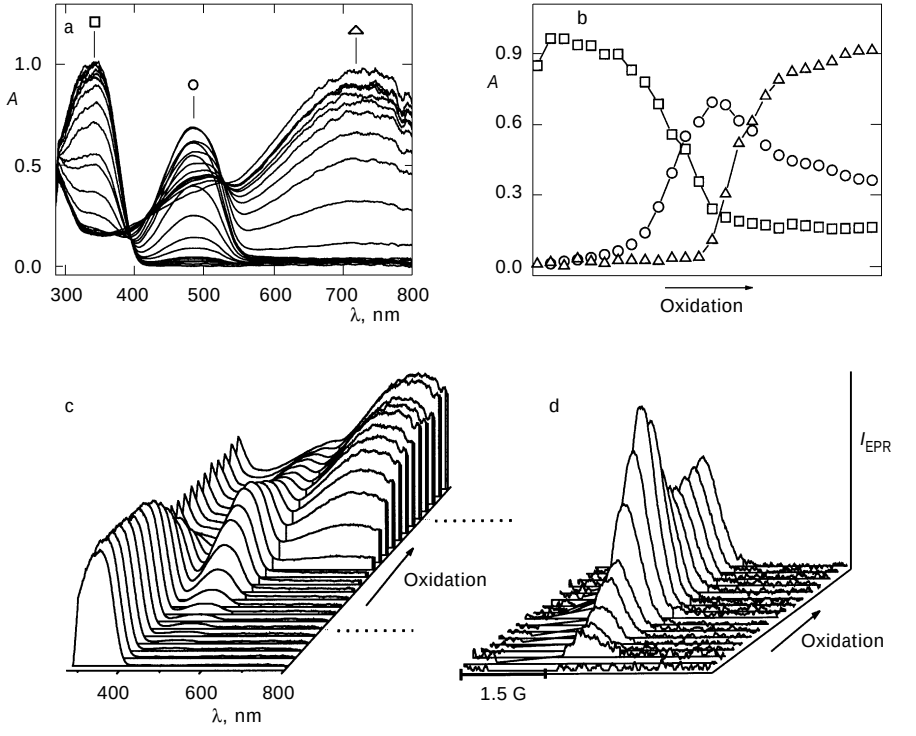

FIG. 5

UV-VIS spectra recorded during the amperometric oxidation of **5** in CH_2Cl_2/0.1 M $TBAPF_6$ on the laminated ITO electrode: a 2D plot; b extracted kinetic curves; c 3D plot, along with d the simultaneously recorded EPR spectra (only the marked region presented, dashed lines)

compound **4** in Fig. 6. The absorption maximum at 350 nm is characteristic of the triphenylamine cation-radical with further two maxima at 550 and 650 nm (ref.[21]). The maxima at 485 and 700 nm are characteristic of tetraarylbenzidine-type compounds. This is in accordance with the anodic route suggested above for **3**, assuming coupling of the initially formed unstable cation-radical under formation of its dimeric form and further oxidation to the mono- and dication. This route, suggested for **3**, is also valid for **4**. Whereas here the primary formation of two independent redox centres in the structure of **4** is assumed, the dimerization in solution could be an alternative pathway.

The energy of the HOMO levels of the investigated compounds can be determined from the oxidation half-wave potentials obtained by cyclovoltammetric measurements in solution. The oxidation half-wave potential for compound **5** has been determined as +0.29 V *vs* Fc/Fc^+. Assuming that the HOMO energy for the ferrocene/ferricenium standard is –4.8 eV

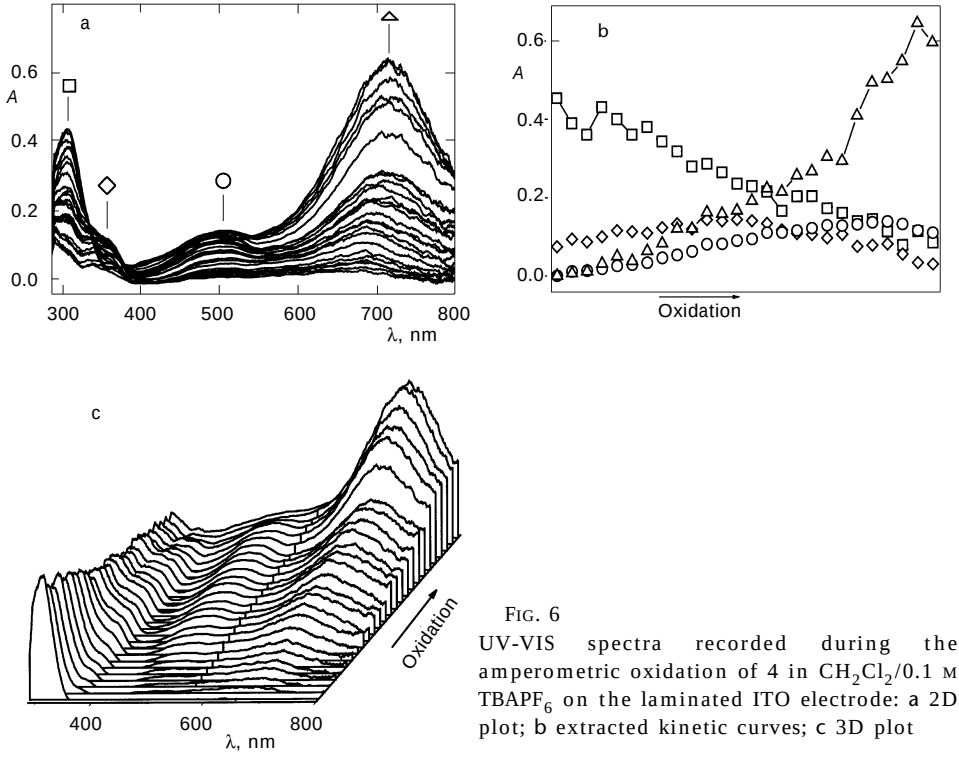

FIG. 6
UV-VIS spectra recorded during the amperometric oxidation of 4 in CH_2Cl_2/0.1 M $TBAPF_6$ on the laminated ITO electrode: a 2D plot; b extracted kinetic curves; c 3D plot

with respect to the zero vacuum level, the HOMO energy for compound **5** has been evaluated to –5.09 eV. The energy barrier for hole injection from ITO is therefore expected to be 0.29 V (assuming φ(ITO) = 4.8 eV). The LUMO energetic position for compound **5** has been estimated to be –1.45 eV, based on the energy maximum of the solution absorption band. The HOMO-LUMO gap is then 3.64 eV.

CONCLUSIONS

Fluorenylidene-linked triarylamines have been prepared by the palladium-catalyzed Hartwig–Buchwald amination. These linked triarylamines, when compared with the low-molecular-weight analogues conventionally used in OLEDs, show greatly increased glass-transition temperatures while their desirable electronic characteristics is preserved. EPR investigations generally confirmed that for all investigated compounds, in the region of the first oxidation peak, paramagnetic species are formed which are cation-radicals. In the model compounds (**1**, **2**, and **3**), the hyperfine splittings (quintet 1 : 2 : 3 : 2 : 1) indicate the formation of species with two equivalent nitrogen atoms, that well correspond to tetraarylbenzidine cations. In the newly prepared compounds **4** and **5**, only unresolved broad single lines were observed; however, from the UV-VIS spectroelectrochemical results it can be concluded that these spectra are individual tetraarylbenzidine cations linked with non-conjugated fluorene bridges. The UV-VIS bands at about 480 nm and the EPR kinetic curves passed through a maximum in the region of the first oxidation peak and decreased in the region of the second peak. This confirms that in the second oxidation step, EPR-silent dicationic species are formed from all investigated compounds (of both monomeric and dimeric type). The cyclovoltammetric investigations combined with EPR and UV-VIS measurements presented here provide evidence that compound **5** could be used as an efficient material for hole transport in OLEDs. These investigations as well as the synthesis of further fluorene-linked compounds are currently under way.

Financial support from the Bayerische Forschungsstiftung (R. F.), the Fonds der Chemischen Industrie (G. F. M.), the Bayerischer Forschungsverbund Katalyse (FORKAT), the Deutsche Forschungsgemeinschaft, the Deutscher Akademischer Austauschdienst (P. R.), the BMBF and the Slovak Grant Agency (Project VEGA 1/4206/97), is gratefully acknowledged. We thank Dipl.-Chem. T. Braig for helpful discussions.

REFERENCES

1. Tang C. W., Van Slyke S. A.: *Appl. Phys. Lett.* **1987**, *51*, 913.
2. Adachi Ch., Nagai K., Tamoto N.: *Appl. Phys. Lett.* **1995**, *66*, 2679.
3. Van Slyke S. A., Chen C. H., Tang C. W.: *Appl. Phys. Lett.* **1996**, *69*, 2160.
4. Adachi C., Tsutsui T., Saito S.: *Appl. Phys. Lett.* **1989**, *55*, 1489.
5. Shirota Y., Kobata T., Noma N.: *Chem. Lett.* **1989**, 1145.
6. Inada H., Ohnishi K., Nomura S., Higuchi A., Nakano H., Shirota Y.: *J. Mater. Chem.* **1994**, *4*, 171.
7. Koene B. E., Loy D. E., Thompson M. E.: *Chem. Mater.* **1998**, *10*, 2235.
8. O'Brien D. F., Burrows P. E., Forrest S. R., Koene B. E., Loy D. E., Thompson M. E.: *Adv. Mater. (Weinheim, Ger.)* **1998**, *10*, 1108.
9. Salbeck J., Yu N., Bauer J., Weissörtel F., Bestgen H.: *Synth. Met.* **1997**, *91*, 209.
10. Bach U., Lupo D., Comte P., Moser J. E., Weissörtel F., Salbeck J., Spreitzer H., Grätzel M.: *Nature* **1998**, *395*, 583.
11. Salbeck J., Weissörtel F., Bauer J.: *Macromol. Symp.* **1997**, *125*, 121.
12. Kido J., Komada M., Harada G., Nagai K.: *Polym. Adv. Technol.* **1995**, *17*, 703.
13. Park K. H., Tani T., Kakimoto M.-A., Imai Y.: *Macromol. Chem. Phys.* **1998**, *199*, 1029.
14. Korshak V. V., Vinogradova S. V., Vygodskii Y. S.: *J. Macromol. Sci., Part C* **1974**, *11*, 45.
15. Thelakkat M., Fink R., Haubner F., Schmidt H.-W.: *Macromol. Symp.* **1997**, *125*, 157.
16. Seo E. T., Nelson R. F., Fritsch J. M., Marcoux L. S., Leedy D. W., Adams R. N.: *J. Am. Chem. Soc.* **1966**, *5*, 3498.
17. Anderson J. D., McDonald E. M., Lee P. A., Anderson M. L., Ritchie E. L., Hall H. K., Hopkins T., Mash E. A., Wang J., Padias A., Thayumanavan S., Barlow S., Marder S. R., Jabbour G. E., Shaheen S., Kippelen B., Peyghambarian N., Wightman R. M., Armstrong N. R.: *J. Am. Chem. Soc.* **1998**, *120*, 9646.
18. Creason S. C., Wheeler J., Nelson R. F.: *J. Org. Chem.* **1972**, *37*, 4440.
19. Marcoux L. S., Adams R. N., Feldberg S. W.: *J. Phys. Chem.* **1969**, *73*, 2611.
20. Debrodt H., Heusler K. E.: *Z. Phys. Chem. (Munich)* **1981**, *125*, 35.
21. Sumiyoshi T.: *Chem. Lett.* **1995**, 645.
22. Oyama M., Nozaki K., Okazaki S.: *Anal. Chem.* **1991**, *63*, 1387.
23. Okutsu S., Onikubo T., Tamano M., Enokida T.: *IEEE Trans. Electron Devices* **1997**, *44*, 1302.
24. Driver M. S., Hartwig J. F.: *J. Am. Chem. Soc.* **1996**, *118*, 7217.
25. Wolfe J. P., Wagaw S., Buchwald S. L.: *J. Am. Chem. Soc.* **1996**, *118*, 7215.
26. Louie J., Hartwig J. F.: *J. Am. Chem. Soc.* **1997**, *119*, 11695.
27. Tanaka H., Tokito S., Taga Y., Okada A.: *Chem. Commun.* **1996**, 2175.
28. Thelakkat M., Schmidt H.-W.: *Adv. Mater. (Weinheim, Ger.)* **1998**, *10*, 219.
29. Katsuma K., Shirota Y.: *Adv. Mater. (Weinheim, Ger.)* **1998**, *10*, 223.
30. Pommerehne J., Westweber H., Guss W., Mahrt R. F., Bässler H., Porsch M., Daub J.: *Adv. Mater. (Weinheim, Ger.)* **1995**, *7*, 551.
31. Neudeck A., Kress L.: *J. Electroanal. Chem.* **1998**, *437*, 141.
32. Rapta P., Neudeck A., Petr A., Dunsch L.: *J. Chem. Soc., Faraday Trans.* **1998**, *94*, 3625.
33. Yamamoto T., Nishiyama M., Koie Y.: *Tetrahedron Lett.* **1998**, *39*, 2367.
34. Veregin R. P., Harbour J. R.: *J. Phys. Chem.* **1990**, *94*, 6231.
35. Neugebauer F. A., Bamberger S., Groh R.: *Chem. Ber.* **1975**, *108*, 2406.